Critical Dynamics of the Anderson Transition on Small-World Graphs

Weitao Chen,[1,2,3] Ignacio García-Mata,[4,5] John Martin,[6] Jiangbin Gong,[1,2,3]
Bertrand Georgeot,[7] and Gabriel Lemarié[2,3,1,7,8,*]
[1]*Department of Physics, National University of Singapore, Singapore*
[2]*MajuLab, CNRS-UCA-SU-NUS-NTU International Joint Research Unit, Singapore*
[3]*Centre for Quantum Technologies, National University of Singapore, Singapore*
[4]*Instituto de Investigaciones Físicas de Mar del Plata (IFIMAR), CONICET–UNMdP, Funes 3350, B7602AYL Mar del Plata, Argentina*
[5]*Consejo Nacional de Investigaciones Científicas y Tecnológicas (CONICET), Mar del Plata, Argentina*
[6]*Institut de Physique Nucléaire, Atomique et de Spectroscopie, CESAM, University of Liège, B-4000 Liège, Belgium*
[7]*Université Toulouse, CNRS, Laboratoire de Physique Théorique, Toulouse, France*
[8]*Université Côte d'Azur, CNRS, INPHYNI, France*

(Received 24 February 2025; revised 26 January 2026; accepted 14 April 2026; published 29 April 2026)

The Anderson transition on random graphs is a paradigm for understanding high-dimensional quantum phase transitions driven by disorder and closely mirrors several features of many-body localization. In this Letter, we introduce a unitary Anderson model on small-world graphs, enabling large-scale, long-time simulations of wave-packet dynamics. This allows us to uncover logarithmically slow critical dynamics, two distinct localization times, and a crossover to ergodic diffusion. Finite-time scaling reveals distinct critical exponents, establishing a dynamical universality class for this exotic transition. Our model opens the way to an experimental realization of the Anderson transition on random graphs in quantum simulators. By combining disorder, high dimensionality, and dynamics, our approach provides a general framework for probing universal features of out-of-equilibrium quantum phase transitions, including those relevant to many-body localization.

DOI: 10.1103/tyrf-2yf7

Introduction—The Anderson transition is a paradigmatic disorder-driven metal-insulator transition rooted in quantum interference [1–5]. Its properties in low-dimensional systems are well understood—extensively characterized as a second-order phase transition in theory [5–8], numerics [9–17], and experiments [18–27].

By contrast, its critical behavior in the high-dimensional limit remains debated [28–30]. The Anderson transition in infinite dimensions (AT^∞) lies outside conventional theories, with strong disorder playing a dominant role [29,31–34]. Early studies focused on the Bethe lattice [35–43], while recent work turned to effectively infinite-dimensional random graphs—random regular graphs and small-world graphs—motivated by their connection to the Fock-space structure of the many-body localized (MBL) phase [44–47].

The MBL transition itself is an ergodic-nonergodic transition in interacting, isolated quantum systems [48–50]. Insights from Anderson models on random graphs have aided MBL studies and vice versa [47,51–66]. Worth mentioning, while random-graph models emulate the complex network structure of Fock space [47,67], they lack important ingredients such as disorder correlations that generate nontrivial effects in the full MBL problem [63,68]. Both transitions face similar ambiguities due to severe finite-size and time effects: the possible existence of a nonergodic delocalized phase and the precise critical properties of the Anderson transition [34,43,52–54,69–87], as well as the critical disorder and nature of the MBL transition [88–102]. Central to the present study is the challenging characterization of the extremely slow dynamics in the vicinity of these transitions [47,51,68,92,103,104].

In parallel, experiments now probe these regimes directly. Cold-atom platforms have enabled studies of MBL [105–108], while digital quantum simulators can now access disordered dynamics with more than 100 qubits [109]. Single-particle localization on engineered random graphs has also become feasible through quantum-circuit architectures [110,111], bringing theoretical models and experimental implementations into closer alignment.

Complementing this progress, finite-time scaling has emerged as a powerful tool for extracting critical behavior directly from dynamics [20,75,76,99,112–116]. Wave-packet dynamics, in particular, allow access to critical spreading behavior in both cold atoms and classical waves [19–21]. Finite-time scaling has already been used to extract exponents in three and four dimensions [17,20,21,117,118], but a systematic dynamical theory for AT^∞ remains absent despite substantial progress in eigenstate analyses.

*Contact author: gabriel.lemarie@cnrs.fr

In this Letter, we fill this gap by introducing a Floquet Anderson model on small-world graphs, a variant of the paradigmatic quantum kicked rotor model of quantum chaos [119–122], which enables large-scale simulations of long-time dynamics in the effectively infinite-dimensional limit. By tracking wave-packet spreading, we identify key dynamical signatures of criticality, including logarithmically slow dynamics and multiple localization scales. A finite-time scaling analysis reveals the onset of ergodicity beyond the transition and yields critical exponents consistent with, and extending, results obtained from static observables. Our findings thus lay a dynamical foundation for characterizing the AT$^\infty$ transition. More broadly, the methodology developed here provides a general framework that should be applicable to disordered, high-dimensional systems, with potential relevance to many-body localization, and may help uncover universal features of their anomalous dynamical regimes.

Unitary Anderson model on small-world graphs—We construct our unitary Anderson model on small-world graphs by generalizing the well-known quantum kicked rotor (QKR) [119–122], a paradigmatic model of quantum chaos that exhibits dynamical localization. The Floquet operator $U = U_2 U_1$ consists of two parts: U_1 is the evolution operator of the QKR, incorporating random on-site phases and hopping on a one-dimensional (1D) ring of size N controlled by the kicking parameter K; U_2 implements random two-site unitaries, resulting in $\lfloor pN \rfloor$ long-range links with $0 < p < 1/2$, that generate small-world connectivity. Together, they define a QKR living on a small-world graph with infinite dimensionality. We provide a detailed explanation of this model in Appendix A.

Single-particle models on random graphs, such as the one introduced here, often serve as effective toy models for many-body systems, where the Hilbert space exhibits an emergent graph structure. This connection has provided valuable insights into the MBL problem [47,51–66]. The kicked unitary nature of our model enables large-scale exact diagonalization via polynomial filtering techniques [123], allowing accurate finite-size scaling of eigenstate and spectral properties. For $p = 0.1$, we pinpoint the critical point at $K_c \approx 1.95$ and characterize the critical behavior, in agreement with prior results [52–54]; full details will be presented elsewhere [124]. Additionally, the Floquet structure makes the model well suited for quantum-circuit implementations [111] and a useful simplified setting for studying Floquet MBL, where localization appears under periodic driving [125–127].

Wave-packet dynamics across the Anderson transition in the unitary Anderson model on small-world graphs—The time evolution of wave packets provides a direct probe of the critical dynamical properties—a challenging task due to the need for large system sizes and long evolution times, yet one that we successfully achieve through our model and numerical approach. For a wave function initially localized on a single site, $|\psi(t=0)\rangle = |i_0\rangle$ we define the "average" and "typical" wave packet as $\Pi(r,t) = \langle \sum_{i:d(i,i_0)=r} |\psi(i,t)|^2 \rangle$ and $\Pi_{\mathrm{typ}}(r,t) = \mathcal{N}_{\mathrm{typ}} \langle N(r) \rangle \exp \langle \sum_{i:d(i,i_0)=r} \ln |\psi(i,t)|^2 / N(r) \rangle$, with $\mathcal{N}_{\mathrm{typ}}$ a normalization factor, respectively. The distance $r = d(i,i_0)$ is the graph (or Hamming) distance between site i and the initial site i_0, and the sum runs over the $N(r)$ sites i at distance r from i_0, with $\langle N(r) \rangle \sim m^r$ ($m \approx 1.3$ for $p = 0.1$). We introduce both average and typical wave packets to probe the spatially heterogeneous dynamics of the model. Even within a single realization, the wave-function profile is highly uneven: a few branches carry anomalously large amplitudes, while most carry much smaller ones, see also [53,54,128]. Consequently, the average wave packet is dominated by rare large-amplitude branches, whereas the typical wave packet reflects the behavior of the bulk. This distinction arises from intrinsic spatial heterogeneity within a single sample, rather than from rare disorder realizations. It becomes particularly important in localized or near-localized regimes, where the average profile decays more slowly than the typical one, revealing two characteristic localization scales associated with rare and typical branches.

One of our main findings is the clear distinction between average and typical wave packets, as shown in Fig. 1. This distinction highlights the nonergodic nature of both the localized regime [$K = 1.5$, Figs. 1(a) and 1(d)] and the critical regime [$K = 1.95$, Figs. 1(b) and 1(e)]. It also reveals nonergodic behavior in the delocalized regime [$K = 2.5$, Figs. 1(c) and 1(f)] at times shorter than the ergodic time, which separates nonergodic critical-like dynamics from ergodic transport [53,54]. Beyond average and typical quantities, one could further consider moments of the wave-packet amplitude, $P_q(t) = \sum_i |\psi(i,t)|^{2q}$, and analyze their critical dynamical behavior in a manner similar to previous studies of eigenstates [52–54]. We leave a systematic investigation of $P_q(t)$ for future work [124] and focus here on the distinct behaviors of the average and typical wave packets in the following sections.

Logarithmically slow critical dynamics—The critical dynamics of such highly heterogeneous systems are often ultraslow, similar to those observed in glassy phases [129]. This makes detecting critical behavior particularly challenging, as it requires access to very long timescales and large system sizes. Our unitary model offers a significant advantage in this regard, enabling efficient simulations of long-time dynamics in large systems via fast Fourier transform. At the critical point, the spatial profile decays algebraically $\Pi(r,t) \sim \Pi(0,t) r^{-(1+\mu)}$ for $r < r^*(t)$ and decays rapidly for $r > r^*(t)$, where $r^*(t)$ characterizes the wavefront. From the numerical data shown in Fig. 1(b), we find $\mu = 0.24$ and $r^*(t) \sim \ln t$. These dynamical properties of the wave packet reproduce the "critical localization" behavior predicted by random-matrix models of AT$^\infty$ [75,76], similar to the behavior predicted for random

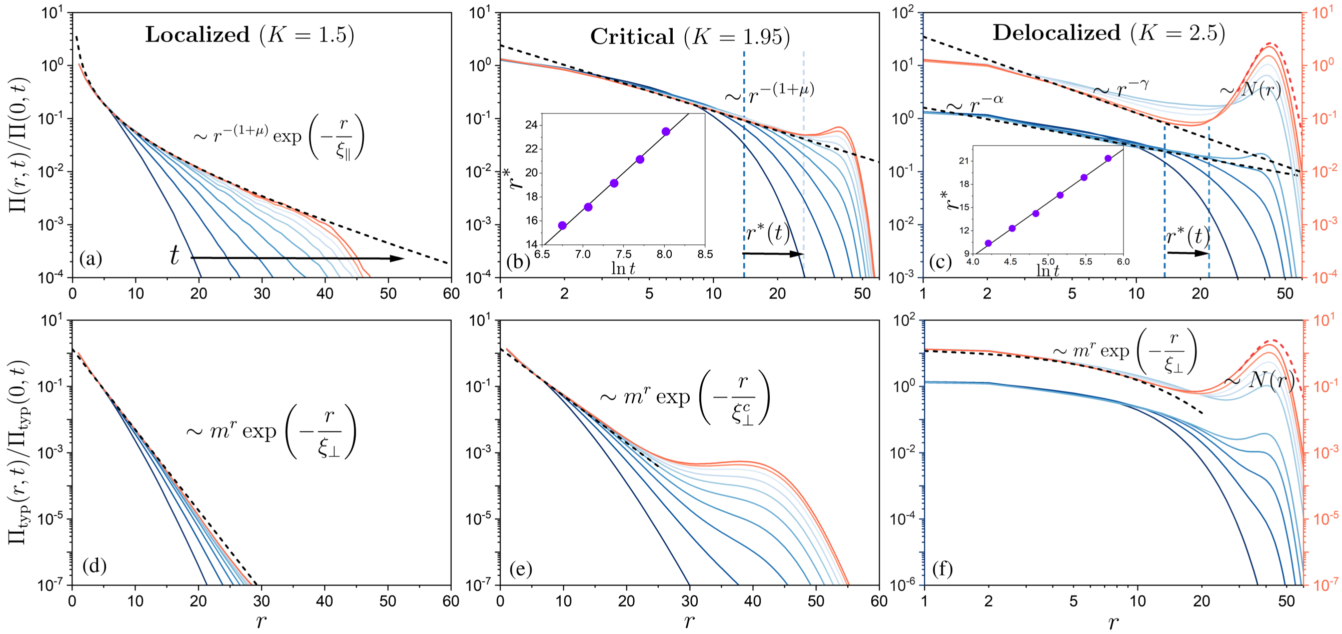

FIG. 1. Wave-packet dynamics across the Anderson transition on small-world graphs: (a)–(c) show the average wave-packet profile $\Pi(r,t)$, while (d)–(f) display the typical wave-packet profile $\Pi_{typ}(r,t)$. Curves from dark blue to pale orange correspond to evolution times $t = 18$, 48, 126, 329, 853, 2212, 5736, 14 873, 38 566, 10^5. A strong distinction between average and typical wave packets emerges in the localized and critical regimes and at times shorter than the ergodic time in the delocalized regime [lower blue curves in (c) and (f)], highlighting nonergodicity. Notably, the typical wave packet saturates after the short typical localization time τ_{loc}^{typ} [see also Fig. 2(b), inset], forming an exponentially localized profile with localization length $\xi_\perp$, even at criticality. Conversely, the average wave packet exhibits slow logarithmic dynamics, a power-law spatial decay at criticality, and much slower convergence with exponential localization in the localized regime. Black dashed lines represent theoretical fits. Blue dashed lines in (b) and (c) indicate the wavefront r^*, marking deviations from power-law decay, with insets showing $r^* \sim \ln t$. Red dashed lines in (c) and (f) highlight the spatially ergodic behavior at large times and distances in the delocalized regime. In (c) and (f), the first five short-time curves are shifted vertically (blue y axis), while the long-time curves align with the red y axis for clarity. Results are averaged over 5400 disorder realizations with $N = 2^{19}$ and $p = 0.1$.

regular graphs (with $\mu = 0.5$) [73]. The spatial profile of the typical wave packet shown in Fig. 1(e) is distinct from the average one and converges after a finite typical localization time τ_{loc}^{typ} [see inset of Fig. 2(b)] to an exponentially localized profile with the finite localization length $\xi_\perp^c \approx (2 \ln m)^{-1}$, i.e., $\Pi_{typ}(r,t)/\Pi_{typ}(0,t) \sim m^r e^{-r/\xi_\perp^c}$, in agreement with Refs. [53,54].

The critical behavior is also encoded in the dynamics of the return probability, $\Pi(0,t)$, which is predicted to decay as $\Pi_c(0,t) \sim (\ln t)^{-\mu} + \Pi_c(0,\infty)$ [53,72,75,76]. To mitigate fluctuations and considering the relationship between $\Pi(0,t)$ and the inverse participation ratio P_2 of eigenstates at large times, it is important to work with coarse-grained wave packets, starting from an initial flat distribution over $N_{init} > 1$ sites. In Fig. 2(a), we show the return probability of coarse-grained wave packets initialized as $|\psi(t=0)\rangle = \sum_{i_0=1}^{N_{init}} (e^{i\phi_{i_0}}/\sqrt{N_{init}})|i_0\rangle$, where ϕ_{i_0} are independent random phases that we average over, and $N_{init} = 32$. The lowest curve represents $\Pi_c(0,t)$ for system size $N = 2^{17}$ and large evolution times up to $t = 10^5$ and is found compatible with the predicted behavior with $\mu = 0.24$ [determined from Fig. 1(b)] and a small fitted value $\Pi_c(0,\infty) \approx 0.1$.

Localized dynamics and finite-time scaling hypothesis—The localized phase exhibits pronounced nonergodic properties [53,54], as reflected in the distinct spatial profiles of the average and typical wave packets [see Figs. 1(a) and 1(d)]. The average wave packet converges slowly, after an average localization time τ_{loc}, to a profile given by the critical wave packet multiplied by an exponential decay governed by the average localization length $\xi_\parallel$, i.e., $\Pi(r,\infty)/\Pi(0,\infty) \sim r^{-(1+\mu)} e^{-r/\xi_\parallel}$. In this sense, τ_{loc} controls the onset of exponential localization of the average wave packet, and this characteristic time—together with the associated length scale $\xi_\parallel$—diverges at the transition (see Fig. 2).

On the other hand, the typical wave packet rapidly adopts, after a small typical τ_{loc}^{typ} that saturates at a finite value at the transition, a purely exponential localized profile with decay controlled by $\xi_\perp \ll \xi_\parallel$, specifically, $\Pi_{typ}(r,\infty)/\Pi_{typ}(0,\infty) \sim m^r e^{-r/\xi_\perp}$. These observations strongly corroborate the existence of two distinct localization lengths [29,53,54,75,76,124,130], but also reveal the existence of two localization times.

To characterize the divergence of τ_{loc} near criticality, we perform a finite-time scaling analysis of the return

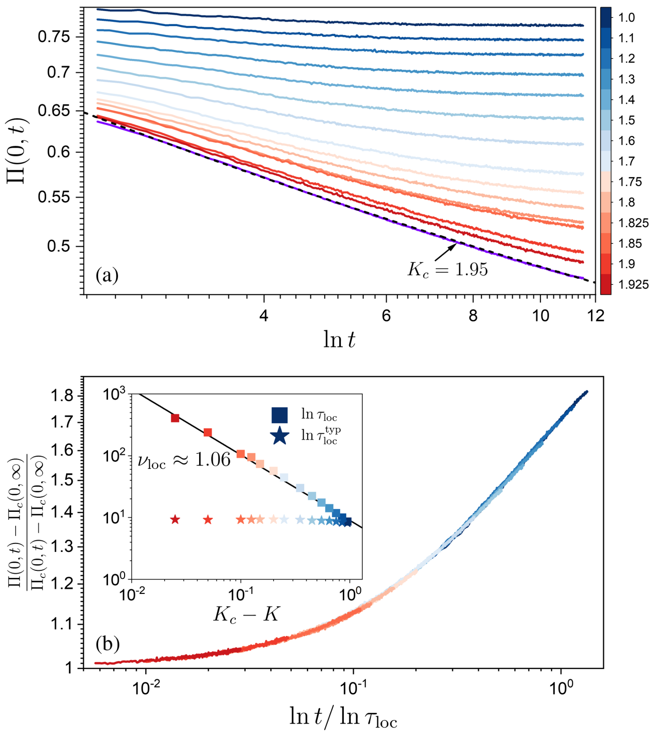

FIG. 2. Finite-time scaling of the return probability $\Pi(0,t)$ in the localized phase of the Anderson transition on small-world graphs. K varies from $K = 1.0$ (strongest localization, upper blue) to $K = 1.95$ (critical, lower purple curve), with evolution times ranging from $t = 10$ to $t = 10^5$. (a) Raw data for the coarse-grained $\Pi(0,t)$ (see text) show a slow convergence to a finite value, indicating asymptotic localization. At the critical point $K_c = 1.95$, the return probability $\Pi_c(0,t)$ decays logarithmically as $\Pi_c(0,t) \approx A(\ln t)^{-\mu} + \Pi_c(0,\infty)$ (black dashed line), with $\mu = 0.24$ (fixed) and $A, \Pi_c(0,\infty) \approx 0.107$ as fitting parameters, signaling critical localization. (b) Single-parameter scaling of $\Pi(0,t)$. The data in (a) collapse onto a single scaling function when plotted as $\ln t/\ln \tau_{\mathrm{loc}}$, where τ_{loc} is the average localization time. The inset shows $\ln \tau_{\mathrm{loc}}$ vs K, along with the typical localization time $\tau_{\mathrm{loc}}^{\mathrm{typ}}$, defined as the time beyond which $\Pi_{\mathrm{typ}}(r = 20, t)$ saturates [see Figs. 1(d) and 1(e)]. While $\tau_{\mathrm{loc}}^{\mathrm{typ}}$ saturates at a finite value at the transition, the average localization time logarithm diverges algebraically as $\ln \tau_{\mathrm{loc}} \sim |K - K_c|^{-\nu_{\mathrm{loc}}}$ with $\nu_{\mathrm{loc}} \approx 1.06$, in perfect agreement with the critical exponent $\nu = 1$ for averaged observables in the localized phase. Results are averaged over 3600–18000 disorder configurations for a system size $N = 2^{17}$ and for $p = 0.1$.

probability $\Pi(0,t)$. In the infinite-time limit, $\Pi(0,\infty) \simeq P_2 \approx \xi_{\parallel}^{-\mu} + P_2^{\infty}$ [59,116,124]. Drawing an analogy with the finite-size scaling of eigenstate moments, we propose the following finite-time scaling behavior for the dynamics [17,52,54,117,118,124]:

$$\frac{\Pi(0,t) - \Pi_c(0,\infty)}{\Pi_c(0,t) - \Pi_c(0,\infty)} = F\left(\frac{\ln t}{\ln \tau_{\mathrm{loc}}}\right), \tag{1}$$

with $F(X) \to 1$ for $X \ll 1$ and $F(X) \to cX^{\mu}$ for $X \gg 1$. This scaling law in $\ln t/\ln \tau_{\mathrm{loc}}$ is analogous to the linear finite-size scaling in $\ln N/\xi_{\parallel}$ found in [53,54,72,124] as times scale like volumes. In Fig. 2(b), we present the collapse of numerical data when plotted with respect to $\ln t/\ln \tau_{\mathrm{loc}}$, revealing a divergence behavior of $\ln \tau_{\mathrm{loc}} \sim |K - K_c|^{-\nu_{\mathrm{loc}}}$ with $\nu_{\mathrm{loc}} \approx 1$, in perfect agreement with the critical exponent $\nu = 1$ for averaged observables in the localized phase [52,53,59]. As one of the key results of this Letter, the determination of the critical exponent through finite-time scaling helps identify and confirm the dynamical universality class of this complex quantum system. In fact, logarithmically slow dynamics have also been observed in MBL systems, though their interpretation remains more ambiguous in the finite-time regime. In this context, finite-time scaling provides a valuable tool to clarify such behavior and identify critical features of the transition [96].

Delocalized dynamics and ergodicity—In the delocalized regime, the average wave packet [Fig. 1(c)] shows two distinct behaviors over time. (i) At early times, it decays with distance following a power law, similar to critical behavior, but with a different exponent. This regime also features a slowly expanding wavefront, scaling as $\ln t$, and reflects a form of "logarithmic multifractality" [75,76]. (ii) At later times, the wave packet settles into a profile with a nonergodic core that eventually transitions to ergodic behavior at larger distances. This crossover marks the restoration of ergodicity. The typical wave packet [Fig. 1(f)] confirms this picture, showing ergodic spreading at long times, while its early-time differences from the average reveal localized, nonergodic "bubbles."

To quantitatively assess the ergodic time τ_{ergo}, we analyze the return probability $\Pi(0,t)$. Care is needed in its interpretation. First, delocalized dynamics suffers from strong finite-size effects, in addition to the finite-time effects we focus on. To minimize these, we exclude data beyond the time when the results for system sizes $N = 2^{17}$ and $N = 2^{18}$ start to diverge from each other. Second, classical diffusion on small-world graphs exhibits "glassy" relaxation, with the return probability decaying as a stretched exponential at long times, $\Pi(0,t) \sim t^{-1/2} e^{-ct^{\beta_d}}$, where c depends on m [131–133]. Our simulations of classical diffusion on small-world graphs yield $\beta_d \approx 0.61$ (see [124]). This contrasts with the exponential decay found in random regular graphs [72] and Bethe lattice [134].

Based on the picture provided by wave packets, at short times the system resides in a nonergodic bubble, where the return probability decays logarithmically slowly, $\Pi(0,t) \sim (\ln t)^{-d(K)}$ [75,76]. We propose that the quantum decay follows the behavior

$$\Pi(0,t) \sim (\ln t)^{-d(K)} e^{-[t/\tau_{\mathrm{ergo}}(K)]^{\beta_d}}. \tag{2}$$

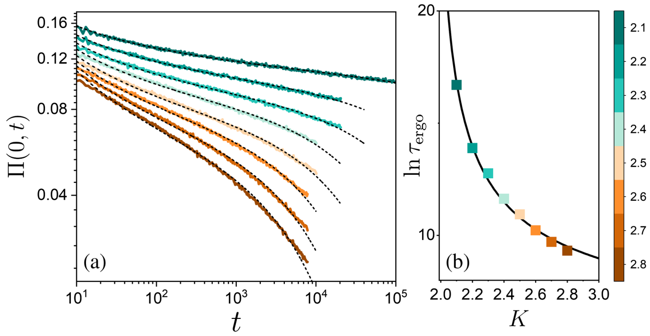

FIG. 3. Ergodic time scaling in the delocalized phase. (a) Time evolution of the return probability $\Pi(0,t)$ for $K = 2.1, 2.2, \ldots, 2.8$ (top to bottom). To minimize finite-size effects, data beyond the point where dynamics for system sizes $N = 2^{17}$ and $N = 2^{18}$ deviate are excluded. The dashed lines represent fits by $A(\ln t)^{-d} \exp[-(t/\tau_{\text{ergo}})^{\beta_d}]$, with $\beta_d = 0.61$ the fixed stretch exponent of classical diffusion on small-world graphs we determined independently, and A, d, τ_{ergo} as fitting parameters. Results are averaged over 18 000 disorder configurations. (b) Dependence of the ergodic time τ_{ergo} on $K > K_c$, extracted from the fits. The solid line shows a fit of the form $A|K - K_c|^{-\nu} + C$, with $\nu = 0.5$ (fixed).

It is important to note that this form of decay is difficult to predict *a priori*. Without direct access to the full spatial distribution of the wave-packet dynamics, the short-time logarithmic decay would be challenging to identify with confidence. In Fig. 3(a), the numerical data are well fitted by this formula, and the ergodic time shown in Fig. 3(b) aligns with the analytical prediction, $\tau_{\text{ergo}}(K) \sim e^{\text{cst}|K-K_c|^{-\nu}}$, with $\nu = 0.5$ [72]. Thus, $\tau_{\text{ergo}}(K)$ behaves as the correlation volume [52,72–74]. Such stretched-exponential forms are also widely observed in MBL systems, often cited as evidence for prethermalization or nonergodicity [135–139]. Our results contribute to demonstrate that a quantum system can remain ergodic despite exhibiting stretched-exponential decay, with an exponent that stays below unity.

Experimental realization—The Floquet-unitary nature of our model makes it feasible to implement using quantum-circuit architectures in modern quantum simulators [140], with the assistance of sequential multicontrolled quantum gates [141] or quantum cellular automata circuits [111]. We refer to Appendix B for a detailed discussion of the experimental realization.

Conclusion—We have explored the dynamical Anderson transition in infinite dimensions by introducing a unitary Anderson model on small-world graphs. This model generalizes the paradigmatic quantum kicked rotor of quantum chaos to an effectively infinite-dimensional setting and allows us to capture the essential features of the Anderson transition in this limit: logarithmically slow spreading at criticality, the emergence of two distinct localization times in the localized phase, and a crossover to ergodic diffusion at large scales and long times in the delocalized regime. Through finite-time scaling, we identify two critical exponents ($\nu_{\text{loc}} \approx 1$ and $\nu \approx 1/2$) characterizing the divergence of localization and ergodic times, respectively. Our approach provides a direct probe of the critical quantum dynamics in complex, disordered systems and introduces robust tools for their systematic analysis. These results not only offer a clear dynamical picture of AT^{∞} in driven, nonequilibrium settings, but also challenge recent conclusions drawn from alternative graph and matrix models [80,81,103,142,143]. Most importantly, this work establishes a methodological framework for dynamical scaling in infinite-dimensional localization, with potential relevance to many-body localization.

Acknowledgments—We wish to thank O. Giraud for fruitful discussions. This study has been (partially) supported through the EUR Grant No. NanoX ANR-17-EURE- 0009 in the framework of the "Programme des Investisse- ments d'Avenir," the France 2030 program (Grant No. ANR-23-PETQ-0002), the French-Argentinian IRP COQSYS, research funding Grants No. ANR-18-CE30-0017, No. ANR-19-CE30-0013, and ManyBodyNet, and by the Singapore Ministry of Education Academic Research Funds Tier II (MOE-T2EP50223-0009 and MOE-T2EP50222-0005). We thank Calcul en Midi-Pyrénées (CALMIP), the National Supercomputing Centre (NSCC) of Singapore, and the Consortium des Equipements de Calcul Intensif (CECI), funded by the Fonds de la Recherche Scientifique de Belgique (F. R. S.-FNRS) under Grant No. 2.5020.11 for computational resources and assistance. W. C. is supported by the President's Graduate Fellowship at National University of Singapore and the Merlion Ph.D. Scholarship awarded by the French Embassy in Singapore. I. G.-M. received support from Argentinian Agencia I + D+i (Grants No. PICT-2020-SERIEA-00740 and No. PICT-2020-SERIEA-01082). J. G. is supported by the National Research Foundation, Singapore through the National Quantum Office, hosted in A*STAR, under its Centre for Quantum Technologies Funding Initiative (S24Q2d0009).

Data availability—The data that support the findings of this article are openly available [144].

[1] P. W. Anderson, Absence of diffusion in certain random lattices, Phys. Rev. **109**, 1492 (1958).

[2] E. Abrahams, *50 years of Anderson Localization* (World Scientific, Singapore, 2010), Vol. 24.

[3] P. A. Lee and T. V. Ramakrishnan, Disordered electronic systems, Rev. Mod. Phys. **57**, 287 (1985).

[4] B. Kramer and A. MacKinnon, Localization: Theory and experiment, Rep. Prog. Phys. **56**, 1469 (1993).

[5] F. Evers and A. D. Mirlin, Anderson transitions, Rev. Mod. Phys. **80**, 1355 (2008).

[6] F. J. Wegner, Disordered system with n orbitals per site: $n = \infty$ limit, Phys. Rev. B **19**, 783 (1979).
[7] K. Efetov, Supersymmetry and theory of disordered metals, Adv. Phys. **32**, 53 (1983).
[8] F. Wegner, Four-loop-order β-function of nonlinear σ-models in symmetric spaces, Nucl. Phys. **B316**, 663 (1989).
[9] M. Schreiber and H. Grussbach, Dimensionality dependence of the metal-insulator transition in the Anderson model of localization, Phys. Rev. Lett. **76**, 1687 (1996).
[10] I. Travěnec and P. Markoš, Critical conductance distribution in various dimensions, Phys. Rev. B **65**, 113109 (2002).
[11] A. M. García-García and E. Cuevas, Dimensional dependence of the metal-insulator transition, Phys. Rev. B **75**, 174203 (2007).
[12] Y. Ueoka and K. Slevin, Dimensional dependence of critical exponent of the Anderson transition in the orthogonal universality class, J. Phys. Soc. Jpn. **83**, 084711 (2014).
[13] K. Slevin and T. Ohtsuki, Corrections to scaling at the Anderson transition, Phys. Rev. Lett. **82**, 382 (1999).
[14] A. Rodriguez, L. J. Vasquez, K. Slevin, and R. A. Römer, Multifractal finite-size scaling and universality at the Anderson transition, Phys. Rev. B **84**, 134209 (2011).
[15] A. Rodriguez, L. J. Vasquez, K. Slevin, and R. A. Römer, Critical parameters from a generalized multifractal analysis at the Anderson transition, Phys. Rev. Lett. **105**, 046403 (2010).
[16] A. Rodriguez, L. J. Vasquez, and R. A. Römer, Multifractal analysis with the probability density function at the three-dimensional Anderson transition, Phys. Rev. Lett. **102**, 106406 (2009).
[17] G. Lemarié, H. Lignier, D. Delande, P. Szriftgiser, and J. C. Garreau, Critical state of the Anderson transition: Between a metal and an insulator, Phys. Rev. Lett. **105**, 090601 (2010).
[18] J.-C. Garreau, Quantum simulation of disordered systems with cold atoms, C.R. Phys. **18**, 31 (2017).
[19] S. Faez, A. Strybulevych, J. H. Page, A. Lagendijk, and B. A. van Tiggelen, Observation of multifractality in Anderson localization of ultrasound, Phys. Rev. Lett. **103**, 155703 (2009).
[20] J. Chabé, G. Lemarié, B. Grémaud, D. Delande, P. Szriftgiser, and J. C. Garreau, Experimental observation of the Anderson metal-insulator transition with atomic matter waves, Phys. Rev. Lett. **101**, 255702 (2008).
[21] M. Lopez, J.-F. Clément, P. Szriftgiser, J. C. Garreau, and D. Delande, Experimental test of universality of the Anderson transition, Phys. Rev. Lett. **108**, 095701 (2012).
[22] T. F. Rosenbaum, K. Andres, G. A. Thomas, and R. N. Bhatt, Sharp metal-insulator transition in a random solid, Phys. Rev. Lett. **45**, 1723 (1980).
[23] M. A. Paalanen, T. F. Rosenbaum, G. A. Thomas, and R. N. Bhatt, Stress tuning of the metal-insulator transition at Millikelvin temperatures, Phys. Rev. Lett. **48**, 1284 (1982).
[24] L. A. Cobus, W. K. Hildebrand, S. E. Skipetrov, B. A. van Tiggelen, and J. H. Page, Transverse confinement of ultrasound through the Anderson transition in three-dimensional mesoglasses, Phys. Rev. B **98**, 214201 (2018).
[25] H. Hu, A. Strybulevych, J. Page, S. E. Skipetrov, and B. A. van Tiggelen, Localization of ultrasound in a three-dimensional elastic network, Nat. Phys. **4**, 945 (2008).
[26] F. Jendrzejewski, A. Bernard, K. Mueller, P. Cheinet, V. Josse, M. Piraud, L. Pezzé, L. Sanchez-Palencia, A. Aspect, and P. Bouyer, Three-dimensional localization of ultracold atoms in an optical disordered potential, Nat. Phys. **8**, 398 (2012).
[27] G. Semeghini, M. Landini, P. Castilho, S. Roy, G. Spagnolli, A. Trenkwalder, M. Fattori, M. Inguscio, and G. Modugno, Measurement of the mobility edge for 3D Anderson localization, Nat. Phys. **11**, 554 (2015).
[28] E. Tarquini, G. Biroli, and M. Tarzia, Critical properties of the Anderson localization transition and the high-dimensional limit, Phys. Rev. B **95**, 094204 (2017).
[29] M. R. Zirnbauer, Wegner model in high dimension: U(1) symmetry breaking and a non-standard phase of disordered electronic matter, I. One-replica theory, arXiv:2309.17323.
[30] B. L. Altshuler, V. E. Kravtsov, A. Scardicchio, P. Sierant, and C. Vanoni, Renormalization group for Anderson localization on high-dimensional lattices, arXiv:2403.01974.
[31] A. D. Mirlin and Y. V. Fyodorov, Distribution of local densities of states, order parameter function, and critical behavior near the Anderson transition, Phys. Rev. Lett. **72**, 526 (1994).
[32] A. D. Mirlin and Y. V. Fyodorov, Statistical properties of one-point Green functions in disordered systems and critical behavior near the Anderson transition, J. Phys. I **4**, 655 (1994).
[33] J. Arenz and M. R. Zirnbauer, Wegner model on a tree graph: U(1) symmetry breaking and a non-standard phase of disordered electronic matter, arXiv:2305.00243.
[34] M. Baroni, G. G. Lorenzana, T. Rizzo, and M. Tarzia, Corrections to the Bethe lattice solution of Anderson localization, Phys. Rev. B **109**, 174216 (2024).
[35] M. R. Zirnbauer, Localization transition on the Bethe lattice, Phys. Rev. B **34**, 6394 (1986).
[36] M. R. Zirnbauer, Anderson localization and non-linear sigma model with graded symmetry, Nucl. Phys. **B265**, 375 (1986).
[37] C. Monthus and T. Garel, Anderson localization on the Cayley tree: Multifractal statistics of the transmission at criticality and off criticality, J. Phys. A **44**, 145001 (2011).
[38] G. Biroli, A. C. Ribeiro-Teixeira, and M. Tarzia, Difference between level statistics, ergodicity and localization transitions on the Bethe lattice, arXiv:1211.7334.
[39] G. Parisi, S. Pascazio, F. Pietracaprina, V. Ros, and A. Scardicchio, Anderson transition on the Bethe lattice: An approach with real energies, J. Phys. A **53**, 014003 (2019).
[40] G. Biroli, A. K. Hartmann, and M. Tarzia, Critical behavior of the Anderson model on the Bethe lattice via a large-deviation approach, Phys. Rev. B **105**, 094202 (2022).
[41] A. De Luca, B. L. Altshuler, V. E. Kravtsov, and A. Scardicchio, Anderson localization on the Bethe lattice: Nonergodicity of extended states, Phys. Rev. Lett. **113**, 046806 (2014).
[42] M. Sonner, K. S. Tikhonov, and A. D. Mirlin, Multifractality of wave functions on a Cayley tree: From root to leaves, Phys. Rev. B **96**, 214204 (2017).

[43] V. Kravtsov, B. Altshuler, and L. Ioffe, Non-ergodic delocalized phase in Anderson model on Bethe lattice and regular graph, Ann. Phys. (Amsterdam) **389**, 148 (2018).

[44] B. L. Altshuler, Y. Gefen, A. Kamenev, and L. S. Levitov, Quasiparticle lifetime in a finite system: A nonperturbative approach, Phys. Rev. Lett. **78**, 2803 (1997).

[45] I. V. Gornyi, A. D. Mirlin, and D. G. Polyakov, Interacting electrons in disordered wires: Anderson localization and low-t transport, Phys. Rev. Lett. **95**, 206603 (2005).

[46] D. Basko, I. Aleiner, and B. Altshuler, Metal–insulator transition in a weakly interacting many-electron system with localized single-particle states, Ann. Phys. (Amsterdam) **321**, 1126 (2006).

[47] K. Tikhonov and A. Mirlin, From Anderson localization on random regular graphs to many-body localization, Ann. Phys. (Amsterdam) **435**, 168525 (2021), special Issue on Localisation 2020.

[48] D. A. Abanin, E. Altman, I. Bloch, and M. Serbyn, Colloquium: Many-body localization, thermalization, and entanglement, Rev. Mod. Phys. **91**, 021001 (2019).

[49] P. Sierant, M. Lewenstein, A. Scardicchio, L. Vidmar, and J. Zakrzewski, Many-body localization in the age of classical computing, arXiv:2403.07111.

[50] B. Collins and I. Nechita, Random matrix techniques in quantum information theory, J. Math. Phys. (N.Y.) **57** (2016).

[51] G. Biroli and M. Tarzia, Delocalized glassy dynamics and many-body localization, Phys. Rev. B **96**, 201114(R) (2017).

[52] I. García-Mata, O. Giraud, B. Georgeot, J. Martin, R. Dubertrand, and G. Lemarié, Scaling theory of the Anderson transition in random graphs: Ergodicity and universality, Phys. Rev. Lett. **118**, 166801 (2017).

[53] I. García-Mata, J. Martin, R. Dubertrand, O. Giraud, B. Georgeot, and G. Lemarié, Two critical localization lengths in the Anderson transition on random graphs, Phys. Rev. Res. **2**, 012020(R) (2020).

[54] I. García-Mata, J. Martin, O. Giraud, B. Georgeot, R. Dubertrand, and G. Lemarié, Critical properties of the Anderson transition on random graphs: Two-parameter scaling theory, Kosterlitz-Thouless type flow, and many-body localization, Phys. Rev. B **106**, 214202 (2022).

[55] N. Macé, F. Alet, and N. Laflorencie, Multifractal scalings across the many-body localization transition, Phys. Rev. Lett. **123**, 180601 (2019).

[56] S. Roy and D. E. Logan, Localization on certain graphs with strongly correlated disorder, Phys. Rev. Lett. **125**, 250402 (2020).

[57] S. Roy and D. E. Logan, Fock-space correlations and the origins of many-body localization, Phys. Rev. B **101**, 134202 (2020).

[58] S. Roy and A. Lazarides, Strong ergodicity breaking due to local constraints in a quantum system, Phys. Rev. Res. **2**, 023159 (2020).

[59] K. S. Tikhonov and A. D. Mirlin, Eigenstate correlations around the many-body localization transition, Phys. Rev. B **103**, 064204 (2021).

[60] G. De Tomasi, I. M. Khaymovich, F. Pollmann, and S. Warzel, Rare thermal bubbles at the many-body localization transition from the Fock space point of view, Phys. Rev. B **104**, 024202 (2021).

[61] S. Roy and D. E. Logan, Fock-space anatomy of Eigenstates across the many-body localization transition, Phys. Rev. B **104**, 174201 (2021).

[62] J. Sutradhar, S. Ghosh, S. Roy, D. E. Logan, S. Mukerjee, and S. Banerjee, Scaling of the fock-space propagator and multifractality across the many-body localization transition, Phys. Rev. B **106**, 054203 (2022).

[63] T. Scoquart, I. V. Gornyi, and A. D. Mirlin, Role of fock-space correlations in many-body localization, Phys. Rev. B **109**, 214203 (2024).

[64] G. Biroli, A. K. Hartmann, and M. Tarzia, Large-deviation analysis of rare resonances for the many-body localization transition, Phys. Rev. B **110**, 014205 (2024).

[65] Z.-H. Sun, Y.-Y. Wang, J. Cui, H. Fan, and M. Heyl, Characterizing dynamical criticality of many-body localization transitions from the Fock-space perspective, arXiv:2405.18188.

[66] J. Niedda, G. B. Testasecca, G. Magnifico, F. Balducci, C. Vanoni, and A. Scardicchio, Renormalization-group analysis of the many-body localization transition in the random-field XXZ chain, Phys. Rev. B 112 (2025).

[67] D. P. Bandeira and M. Tarzia, Anderson localization on husimi trees and its implications for many-body localization, arXiv:2601.04155.

[68] T. Scoquart, I. V. Gornyi, and A. D. Mirlin, Scaling of many-body localization transitions: Quantum dynamics in fock space and real space, Phys. Rev. B **112**, 064203 (2025).

[69] K. S. Tikhonov and A. D. Mirlin, Fractality of wave functions on a Cayley tree: Difference between tree and locally treelike graph without boundary, Phys. Rev. B **94**, 184203 (2016).

[70] A. D. Mirlin and Y. V. Fyodorov, Universality of level correlation function of sparse random matrices, J. Phys. A **24**, 2273 (1991).

[71] Y. Fyodorov, A. Mirlin, and H.-J. Sommers, A novel field theoretical approach to the Anderson localization: Sparse random hopping model, J. Phys. I **2**, 1571 (1992).

[72] K. S. Tikhonov and A. D. Mirlin, Statistics of eigenstates near the localization transition on random regular graphs, Phys. Rev. B **99**, 024202 (2019).

[73] K. S. Tikhonov and A. D. Mirlin, Critical behavior at the localization transition on random regular graphs, Phys. Rev. B **99**, 214202 (2019).

[74] T. Rizzo and M. Tarzia, Localized phase of the Anderson model on the Bethe lattice, Phys. Rev. B **110**, 184210 (2024).

[75] W. Chen, O. Giraud, J. Gong, and G. Lemarié, Quantum logarithmic multifractality, Phys. Rev. Res. **6**, L032024 (2024).

[76] W. Chen, O. Giraud, J. Gong, and G. Lemarié, Describing the critical behavior of the Anderson transition in infinite dimension by random-matrix ensembles: Logarithmic multifractality and critical localization, Phys. Rev. B **110**, 014210 (2024).

[77] V. E. Kravtsov, I. M. Khaymovich, E. Cuevas, and M. Amini, A random matrix model with localization and ergodic transitions, New J. Phys. **17**, 122002 (2015).

[78] V. E. Kravtsov, I. M. Khaymovich, B. L. Altshuler, and L. B. Ioffe, Localization transition on the random regular graph as an unstable tricritical point in a log-normal Rosenzweig-Porter random matrix ensemble, arXiv:2002.02979.

[79] I. M. Khaymovich, V. E. Kravtsov, B. L. Altshuler, and L. B. Ioffe, Fragile extended phases in the log-normal Rosenzweig-Porter model, Phys. Rev. Res. **2**, 043346 (2020).

[80] G. D. Tomasi, M. Amini, S. Bera, I. M. Khaymovich, and V. E. Kravtsov, Survival probability in generalized Rosenzweig-Porter random matrix ensemble, SciPost Phys. **6**, 014 (2019).

[81] I. M. Khaymovich and V. E. Kravtsov, Dynamical phases in a "multifractal" Rosenzweig-Porter model, SciPost Phys. **11**, 045 (2021).

[82] K. S. Tikhonov, A. D. Mirlin, and M. A. Skvortsov, Anderson localization and ergodicity on random regular graphs, Phys. Rev. B **94**, 220203(R) (2016).

[83] B. L. Altshuler, E. Cuevas, L. B. Ioffe, and V. E. Kravtsov, Nonergodic phases in strongly disordered random regular graphs, Phys. Rev. Lett. **117**, 156601 (2016).

[84] P. Sierant, M. Lewenstein, and A. Scardicchio, Universality in Anderson localization on random graphs with varying connectivity, SciPost Phys. **15**, 045 (2023).

[85] M. Pino, Scaling up the Anderson transition in random-regular graphs, Phys. Rev. Res. **2**, 042031(R) (2020).

[86] M. Pino and J. E. Roman, Correlated volumes for extended wave functions on a random-regular graph, Phys. Rev. B **109**, 184204 (2024).

[87] C. Vanoni, B. L. Altshuler, V. E. Kravtsov, and A. Scardicchio, Renormalization group analysis of the Anderson model on random regular graphs, Proc. Natl. Acad. Sci. U.S.A. **121**, e2401955121 (2024).

[88] W. De Roeck and F. Huveneers, Stability and instability towards delocalization in many-body localization systems, Phys. Rev. B **95**, 155129 (2017).

[89] A. Morningstar, L. Colmenarez, V. Khemani, D. J. Luitz, and D. A. Huse, Avalanches and many-body resonances in many-body localized systems, Phys. Rev. B **105**, 174205 (2022).

[90] D. Sels, Bath-induced delocalization in interacting disordered spin chains, Phys. Rev. B **106**, L020202 (2022).

[91] J. Léonard, S. Kim, M. Rispoli, A. Lukin, R. Schittko, J. Kwan, E. Demler, D. Sels, and M. Greiner, Signatures of bath-induced quantum avalanches in a many-body–localized system, arXiv:2012.15270.

[92] F. Weiner, F. Evers, and S. Bera, Slow dynamics and strong finite-size effects in many-body localization with random and quasiperiodic potentials, Phys. Rev. B **100**, 104204 (2019).

[93] J. Šuntajs, J. Bonča, T. c. v. Prosen, and L. Vidmar, Quantum chaos challenges many-body localization, Phys. Rev. E **102**, 062144 (2020).

[94] J. Šuntajs, J. Bonča, T. c. v. Prosen, and L. Vidmar, Ergodicity breaking transition in finite disordered spin chains, Phys. Rev. B **102**, 064207 (2020).

[95] M. Kiefer-Emmanouilidis, R. Unanyan, M. Fleischhauer, and J. Sirker, Slow delocalization of particles in many-body localized phases, Phys. Rev. B **103**, 024203 (2021).

[96] D. Sels and A. Polkovnikov, Dynamical obstruction to localization in a disordered spin chain, Phys. Rev. E **104**, 054105 (2021).

[97] L. Vidmar, B. Krajewski, J. Bonča, and M. Mierzejewski, Phenomenology of spectral functions in disordered spin chains at infinite temperature, Phys. Rev. Lett. **127**, 230603 (2021).

[98] D. Abanin, J. Bardarson, G. De Tomasi, S. Gopalakrishnan, V. Khemani, S. Parameswaran, F. Pollmann, A. Potter, M. Serbyn, and R. Vasseur, Distinguishing localization from chaos: Challenges in finite-size systems, Ann. Phys. (Amsterdam) **427**, 168415 (2021).

[99] P. Sierant, D. Delande, and J. Zakrzewski, Thouless time analysis of Anderson and many-body localization transitions, Phys. Rev. Lett. **124**, 186601 (2020).

[100] R. K. Panda, A. Scardicchio, M. Schulz, S. R. Taylor, and M. Žnidarič, Can we study the many-body localisation transition?, Europhys. Lett. **128**, 67003 (2020).

[101] D. J. Luitz and Y. B. Lev, Absence of slow particle transport in the many-body localized phase, Phys. Rev. B **102**, 100202(R) (2020).

[102] J. Colbois, F. Alet, and N. Laflorencie, Interaction-driven instabilities in the random-field *XXZ* chain, Phys. Rev. Lett. **133**, 116502 (2024).

[103] L. Colmenarez, D. J. Luitz, I. M. Khaymovich, and G. De Tomasi, Subdiffusive Thouless time scaling in the Anderson model on random regular graphs, Phys. Rev. B **105**, 174207 (2022).

[104] H. P. Lüschen, P. Bordia, S. Scherg, F. Alet, E. Altman, U. Schneider, and I. Bloch, Observation of slow dynamics near the many-body localization transition in one-dimensional quasiperiodic systems, Phys. Rev. Lett. **119**, 260401 (2017).

[105] M. Schreiber, S. S. Hodgman, P. Bordia, H. P. Lüschen, M. H. Fischer, R. Vosk, E. Altman, U. Schneider, and I. Bloch, Observation of many-body localization of interacting fermions in a quasirandom optical lattice, Science **349**, 842 (2015).

[106] J.-y. Choi, S. Hild, J. Zeiher, P. Schauß, A. Rubio-Abadal, T. Yefsah, V. Khemani, D. A. Huse, I. Bloch, and C. Gross, Exploring the many-body localization transition in two dimensions, Science **352**, 1547 (2016).

[107] Q. Guo, C. Cheng, Z.-H. Sun, Z. Song, H. Li, Z. Wang, W. Ren, H. Dong, D. Zheng, Y.-R. Zhang *et al.*, Observation of energy-resolved many-body localization, Nat. Phys. **17**, 234 (2021).

[108] T. Kohlert, S. Scherg, X. Li, H. P. Lüschen, S. Das Sarma, I. Bloch, and M. Aidelsburger, Observation of many-body localization in a one-dimensional system with a single-particle mobility edge, Phys. Rev. Lett. **122**, 170403 (2019).

[109] O. Shtanko, D. S. Wang, H. Zhang, N. Harle, A. Seif, R. Movassagh, and Z. Minev, Uncovering local integrability in quantum many-body dynamics, Nat. Commun. **16**, 2552 (2025).

[110] G. Bentsen, T. Hashizume, A. S. Buyskikh, E. J. Davis, A. J. Daley, S. S. Gubser, and M. Schleier-Smith, Treelike interactions and fast scrambling with cold atoms, Phys. Rev. Lett. **123**, 130601 (2019).

[111] E. B. Jones, L. E. Hillberry, M. T. Jones, M. Fasihi, P. Roushan, Z. Jiang, A. Ho, C. Neill, E. Ostby, P. Graf *et al.*, Small-world complex network generation on a digital quantum processor, Nat. Commun. **13**, 4483 (2022).

[112] G. Lemarié, B. Grémaud, and D. Delande, Universality of the Anderson transition with the quasiperiodic kicked rotor, Europhys. Lett. **87**, 37007 (2009).

[113] T. Ohtsuki and T. Kawarabayashi, Anomalous diffusion at the Anderson transitions, J. Phys. Soc. Jpn **66**, 314 (1997).

[114] C. A. Müller, D. Delande, and B. Shapiro, Critical dynamics at the Anderson localization mobility edge, Phys. Rev. A **94**, 033615 (2016).

[115] P. Akridas-Morel, N. Cherroret, and D. Delande, Multifractality of the kicked rotor at the critical point of the Anderson transition, Phys. Rev. A **100**, 043612 (2019).

[116] W. Chen, G. Lemarié, and J. Gong, Critical dynamics of long-range quantum disordered systems, Phys. Rev. E **108**, 054127 (2023).

[117] G. Lemarié, J. Chabé, P. Szriftgiser, J. C. Garreau, B. Grémaud, and D. Delande, Observation of the Anderson metal-insulator transition with atomic matter waves: Theory and experiment, Phys. Rev. A **80**, 043626 (2009).

[118] F. Madani, M. Denis, P. Szriftgiser, J. C. Garreau, A. Rançon, and R. Chicireanu, Exploring quantum criticality in a 4D quantum disordered system, arXiv:2402.06573.

[119] B. V. Chirikov, A universal instability of many-dimensional oscillator systems, Phys. Rep. **52**, 263 (1979).

[120] F. M. Izrailev, Simple models of quantum chaos: Spectrum and eigenfunctions, Phys. Rep. **196**, 299 (1990).

[121] F. L. Moore, J. C. Robinson, C. F. Bharucha, B. Sundaram, and M. G. Raizen, Atom optics realization of the quantum δ-Kicked Rotor, Phys. Rev. Lett. **75**, 4598 (1995).

[122] D. R. Grempel, R. E. Prange, and S. Fishman, Quantum dynamics of a nonintegrable system, Phys. Rev. A **29**, 1639 (1984).

[123] D. J. Luitz, Polynomial filter diagonalization of large Floquet unitary operators, SciPost Phys. **11**, 021 (2021).

[124] W. Chen, I. García-Mata, J. Martin, J. Gong, B. Georgeot, and G. Lemarié (to be published).

[125] P. Ponte, Z. Papić, F. Huveneers, and D. A. Abanin, Many-body localization in periodically driven systems, Phys. Rev. Lett. **114**, 140401 (2015).

[126] D. A. Abanin, W. De Roeck, and F. Huveneers, Theory of many-body localization in periodically driven systems, Ann. Phys. (Amsterdam) **372**, 1 (2016).

[127] A. Haldar and A. Das, Dynamical many-body localization and delocalization in periodically driven closed quantum systems, Ann. Phys. (Berlin) **529**, 1600333 (2017).

[128] B. Derrida and H. Spohn, Polymers on disordered trees, spin glasses, and traveling waves, J. Stat. Phys. **51**, 817 (1988).

[129] J.-P. Bouchaud, L. F. Cugliandolo, J. Kurchan, and M. Mézard, Out of equilibrium dynamics in spin-glasses and other glassy systems, Spin Glasses Random Fields **12**, 9 (1998).

[130] C. Vanoni, B. L. Altshuler, V. E. Kravtsov, and A. Scardicchio, Renormalization group analysis of the Anderson model on random regular graphs (2023).

[131] A. J. Bray and G. J. Rodgers, Diffusion in a sparsely connected space: A model for glassy relaxation, Phys. Rev. B **38**, 11461 (1988).

[132] R. Monasson, Diffusion, localization and dispersion relations on “small-world” lattices, Eur. Phys. J. B **12**, 555 (1999).

[133] S. Jespersen, I. M. Sokolov, and A. Blumen, Relaxation properties of small-world networks, Phys. Rev. E **62**, 4405 (2000).

[134] C. Monthus and C. Texier, Random walk on the Bethe lattice and hyperbolic Brownian motion, J. Phys. A **29**, 2399 (1996).

[135] P. Sierant and J. Zakrzewski, Challenges to observation of many-body localization, Phys. Rev. B **105**, 224203 (2022).

[136] Talia L. M. Lezama, E. J. Torres-Herrera, F. Pérez-Bernal, Y. Bar Lev, and L. F. Santos, Equilibration time in many-body quantum systems, Phys. Rev. B **104**, 085117 (2021).

[137] D. M. Long, Philip J. D. Crowley, V. Khemani, and A. Chandran, Phenomenology of the Prethermal Many-Body Localized Regime, Phys. Rev. Lett. **131**, 106301 (2023).

[138] S. Bera, I. Modak, and R. Moessner, Inhomogeneous Floquet thermalization, Phys. Rev. B **109**, 224206 (2024).

[139] A. Haldar, Kohlrausch regime of slow relaxation and its phenomenology in isolated quantum many-body systems with strong disorder, Phys. Rev. B **111**, 075113 (2025).

[140] E. Altman *et al.*, Quantum simulators: Architectures and opportunities, PRX Quantum **2**, 017003 (2021).

[141] O. Giraud, B. Georgeot, and D. L. Shepelyansky, Quantum computing of delocalization in small-world networks, Phys. Rev. E **72**, 036203 (2005).

[142] S. Bera, G. De Tomasi, I. M. Khaymovich, and A. Scardicchio, Return probability for the Anderson model on the random regular graph, Phys. Rev. B **98**, 134205 (2018).

[143] G. De Tomasi, S. Bera, A. Scardicchio, and I. M. Khaymovich, Subdiffusion in the Anderson model on the random regular graph, Phys. Rev. B **101**, 100201(R) (2020).

[144] W. Chen, I. Garcia-Mata, J. Martin, J. Gong, B. Georgeot, and G. Lemarié, Data for critical dynamics of the Anderson transition on small world graphs, GitHub repository (2025).

[145] D. J. Watts and S. H. Strogatz, Collective dynamics of ’small-world’ networks, Nature (London) **393**, 440 (1998).

[146] E. Hamza, A. Joye, and G. Stolz, Dynamical localization for unitary Anderson models, Math. Phys. Anal. Geom. **12**, 381 (2009).

[147] A. A. Pomeransky and D. L. Shepelyansky, Quantum computation of the Anderson transition in the presence of imperfections, Phys. Rev. A **69**, 014302 (2004).

[148] Y. Yao, L. Xiang, Z. Guo, Z. Bao, Y.-F. Yang, Z. Song, H. Shi, X. Zhu, F. Jin, J. Chen *et al.*, Observation of many-body Fock space dynamics in two dimensions, Nat. Phys. **19**, 1459 (2023).

End Matter

Details on the unitary Anderson model on small-world graphs—We begin with the standard Hamiltonian formulation of the Anderson model on a small-world graph [52–54], defined as $H = \sum_{i=1}^{N} \varepsilon_i |i\rangle\langle i| + \sum_{\langle i,j\rangle} |i\rangle\langle j| + \sum_{k=1}^{\lfloor pN \rfloor} (|i_k\rangle\langle j_k| + |j_k\rangle\langle i_k|)$, where $\{|i\rangle\}$ is the position basis with $1 \le i \le N$, and ε_i are independent identically distributed (i.i.d.) random variables, representing on-site disorder. The second term corresponds to nearest-neighbor hopping on a one-dimensional ring, and the third term introduces long-range hopping links. These long-range links connect pairs of sites (i_k, j_k), randomly chosen with probability $0 < p < 1/2$, resulting in $\lfloor pN \rfloor$ such links. This generates a small-world graph with effective branching number $m \approx (1 + \sqrt{16p + 1}/2)$ [84,145].

To construct the unitary (Floquet) version of this model, we start from the 1D quantum kicked rotor (QKR) [119–122], a paradigmatic model of quantum chaos whose Floquet operator can be interpreted as a unitary Anderson model [146]. The evolution operator over a single period is $U_1 = \sum_{i,j=1}^{N} e^{\mathrm{i}\Phi_i \delta_{ij}} \sum_{k=1}^{N} F_{ik} e^{-\mathrm{i}K\cos(2\pi k/N)} F_{kj}^{-1} |i\rangle\langle j|$, where $F_{jk} = e^{2\pi \mathrm{i} jk/N}/\sqrt{N}$ is the discrete Fourier transform, Φ_i are i.i.d. random phases uniformly distributed over $[0, 2\pi)$, and K is the kicking strength controlling hopping amplitude.

To embed long-range connections and generate small-world structure, we multiply U_1 by unitary two-site gates $U_2^\alpha = (1/\sqrt{2})(|j_\alpha\rangle\langle j_\alpha| + |k_\alpha\rangle\langle k_\alpha| - |j_\alpha\rangle\langle k_\alpha| + |k_\alpha\rangle\langle j_\alpha|) + \sum_{i \ne j_\alpha, k_\alpha} |i\rangle\langle i|$, each acting on a randomly selected pair (j_α, k_α). The total long-range operator is $U_2 = \prod_{\alpha=1}^{\lfloor pN \rfloor} U_2^\alpha$, and the full Floquet operator of our model is $U = U_2 U_1$. Together, U_1 defines the 1D dynamics and U_2 implements small-world long-range connections, forming a small-world graph with infinite dimensionality. As illustrated in Fig. 4, the one-dimensional ring corresponds to the QKR unitary operator U_1, while each long-range link corresponds to a single unitary operator U_2^α.

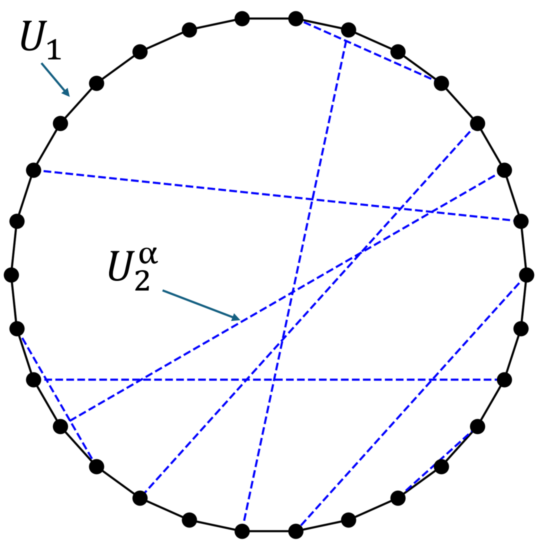

FIG. 4. Illustration of a small-world graph consisting of a 1D ring of N sites (represented by the black circle), on which U_1, the evolution operator of the quantum kicked rotor, acts, characterized by the kicking parameter K. Additionally, there are $\lfloor pN \rfloor$ long-range links, generated by random two-site unitaries U_2^α (blue dashed lines), controlled by the parameter $0 < p < 1/2$. This setup describes a quantum kicked rotor on a random graph with infinite effective dimension and average connectivity $m + 1 \approx (3 + \sqrt{16p + 1}/2)$. It exhibits an Anderson transition driven by the K parameter, between a localized phase for $K < K_c$ and a delocalized phase for $K > K_c$, with critical properties that are universal and independent of the value of $0 < p < 1/2$.

Details on experimental realization—A possible realization scheme was proposed in Ref. [141]. The first part of the Floquet operator U_1, $\sum_{i,j}^{N} e^{\mathrm{i}\Phi_i \delta_{ij}}$, corresponds to on-site random phases Φ_i and can be directly implemented using random phase gates in the computational basis. The second part of U_1, $\sum_{i,j}^{N} \sum_{k=1}^{N} F_{ik} e^{-\mathrm{i}KV(2\pi k/N)} F_{kj}^{-1}$, involves a Fourier transformation and can be implemented using the quantum Fourier transform and its inverse [147]. The realization of U_2 is more involved but remains within reach. One approach generates the small-world shortcuts via a permutation operator P, implemented using a sequence of random controlled-NOT gates acting on randomly chosen qubit pairs (j_α, k_α). This is followed by a multi-controlled rotation gate $C_{i_1,\ldots,i_\mu,\eta_1,\ldots,\eta_\mu,j}(\theta)$, which rotates the jth qubit by angle θ only if each control qubit i_k equals a specified value $\eta_k \in \{0, 1\}$ for $1 \le k \le \mu$, and then by the inverse permutation P^{-1}. This procedure uses only a polynomial number of gates while effectively simulating a Hilbert space of exponential size, benefiting from quantum speedup [141]. Alternatively, the small-world structure can be engineered using quantum cellular automata (QCA) circuits, where mutual information between qubits naturally develops a small-world network after several QCA cycles, as recently demonstrated on a 23-qubit superconducting quantum processor [111]. Both localized and delocalized regimes of our model can be realized with current platforms, while accessing the critical regime may require extended coherence times due to the long-time dynamics. Beyond exact realizations, interacting chains with similar Hilbert-space graph structures can be engineered in cold-atom and programmable quantum simulator platforms [110,148].